# Two-step crosslinking to enhance the printability of methacrylated gellan gum biomaterial ink for extrusion-based 3D bioprinting

Hatai Jongprasitkul [a], Sanna Turunen [a,b], Vijay Singh Parihar [a,*], Minna Kellomäki [a]

[a] *Biomedical and Tissue Engineering Group, BioMediTech, Faculty of Medicine and Health Technology, Tampere University, 33720, Tampere, Finland*
[b] *Brinter Limited, 20520, Turku, Finland*

## ARTICLE INFO

## ABSTRACT

Photocrosslinkable bioinks have gained interest in 3D bioprinting due to their versatility and ease of use. However, a specific functional group, such as methacrylate or photo-click chemistry, is needed in the polymer backbone to enable photocrosslinking. Methacrylated gellan gum (GGMA) precursor has been proven to possess good rheological properties for an injectable hydrogel due to its inherent viscosity. It can also be photo-crosslinked *in situ* at the target site. Unfortunately, the GGMA precursors alone are unable to maintain a stable filament shape after extrusion from the nozzle. In this study, a two-step crosslinking technique involving ionic and photocrosslinking was used to make the GGMA biomaterial ink printable. In the presence of an ionic crosslinker ($Ca^{2+}$), GGMA transformed from a liquid precursor to a weak extrudable hydrogel followed by photocrosslinking turning the weak hydrogel into true hydrogel with good shape fidelity. The printability of various GGMA ink compositions was prescreened thoroughly by characterising their fibre formation and rheological properties. A quantitative approach was introduced to quantify the experimental printability of different GGMA/$CaCl_2$ ink compositions from the printed two-layered grid structures. According to the results, 2% GGMA with 90 mM calcium chloride provided a formulation with the best printability. The optimum ink formulation was then used to print 3D structures. This optimised GGMA ink was printed with consistent fibres and provided high printability during the fabrication. The 3D printed structures still lacked high resolution compared to the control structures. In conclusion, the two-step crosslinking technique provided biomaterial ink with good printability and enabled the printing of genuine 3D constructs. Hence, pre-crosslinked GGMA may be applicable for a wide range of bioprinting applications.

## 1. Introduction

Extrusion-based bioprinting requires bioinks, which are mostly made of soft hydrogels or water-soluble polymers [1,2]. The development of such bioinks must meet specific requirements for fluid properties such as viscosity, shear-thinning, layer stackability and cell encapsulation [3–5]. The choice of bioink depends on the application in question (e.g., soft/hard tissues, biosensors) [6]. So far, hydrogel precursors have been the most used material choice of bioinks for extrusion-based 3D bio-printers due to their biocompatibility, high hydrophilicity, cell-friendly characteristics (promotion of cell growth and cell attachment), and tunability of mechanical properties. However, in order to create suitable hydrogels for extrusion-based bioprinting, the printability and cell sur-vivability must be optimised throughout the printing process [7–10].

As the specialised materials suited for bioprinting have become an important research field, it has come relevant to define the terminology bit further. Groll et al. have clearly defined the terms bioink and biomaterial ink [11,12]. According to their definition, cells are a mandatory component of a bioink. Hence, aqueous compositions of polymers or hydrogel precursors that may include biologically active molecules but without living cells are not considered bioinks but instead biomaterial inks [12]. In our study, we use the term biomaterial ink (in short, "ink") for the material formulations as we have not yet formulated the materials with living cells.

The properties of Gellan gum (GG) can be modified to suit 3D bio-printing applications [13]. These properties, including molecular weight, polymer concentration and the type of crosslinker, affect the characteristics of GG hydrogels [14]. For biofabrication purposes, the GG chain is commonly functionalised with methacrylate groups (MA) to transform it photocrosslinkable and enable mechanical tunability of the

---

hydrogel [15–17]. Methacrylated GG (GGMA) precursor has shown good rheological properties to be used as an injectable hydrogel, so assumably it also suits bioprinting [18].

Unfortunately, the GGMA precursors alone lack the stability to maintain the 3D structure, although the prescreening results based on the rheological data, Power-law modelling, and filament formation imply that the material is extrudable. In fact, it has become clear that prescreening of printability does not provide sufficient data to predict the quality of printing outcome, although it is an important first step in the process of developing and characterising new bioinks for extrusion-based 3D bioprinting [5,15].

According to previously published research studies, gellan gum/ GGMA is usually mixed with materials having good shear-thinning properties, such as chitosan, gelatin or synthetic polymers, to achieve good shape fidelity during the printing process [14,16,17]. The blending of bioink with other materials makes the preparation more complex, is time-consuming, and can yield bath-to-batch variations of each polymer. Moreover, a bioink without blending or stand-alone bioink could bridge the gap between academia and industry, as it offers versatility in both research and commercialisation.

To overcome these challenges, we present here a two-step cross-linking approach, which turns unprintable GGMA into fibre-forming, stackable biomaterial ink capable of forming 3D hydrogel constructs via extrusion-based 3D bioprinting.

In our study, we applied a pre-crosslinking approach (physical crosslinking with $Ca^{2+}$) via coordination bonding of carboxylate groups to calcium ions, providing sufficient stability to maintain the shape before photocrosslinking [19]. The previously published studies have shown that GGMA precursor has an ability to transform from solution to weak hydrogel under low temperature, pH and ionic conditions [13,20, 21]. However, the physically crosslinked GG hydrogels alone cannot maintain their stability *in vivo* after implantation due to the exchange of divalent cations with monovalent ones present at higher concentrations in the physiological environment [20,22]. Thus, we hypothesised that the introduction of two-step crosslinking would improve the printability and printing resolution of the low polymer content GGMA compared to photocrosslinking alone. The two-step crosslinking protocol with ions and UV light was applied to maintain the shape fidelity and printing resolution during the printing at room temperature.

We highlighted the relationship between the two-step crosslinking technique and the printing outcome through stepwise printability evaluations. Therefore, we investigated the parameters that influence printability, including polymer concentration, degree of calcium ionic crosslinking, and UV irradiation time. Different GGMA and calcium chloride ink mixtures were evaluated through three steps: 1) pre-screening printability and rheological profiles, 2) printing parameters, and 3) post-printing analysis. The ink formulations were evaluated for their fibre formability, and the semi-quantitative measurement of 3D printed structures was used to obtain the highest printing resolution. Then, the optimised biomaterial ink was selected to print 3D structures to assess the printing accuracy and swelling behaviour after printing. The study provided a systematical approach to succeed 3D constructs using two-step crosslinking in GGMA inks. We also proposed simple quantitative tests to obtain a high aspect ratio from different ink compositions.
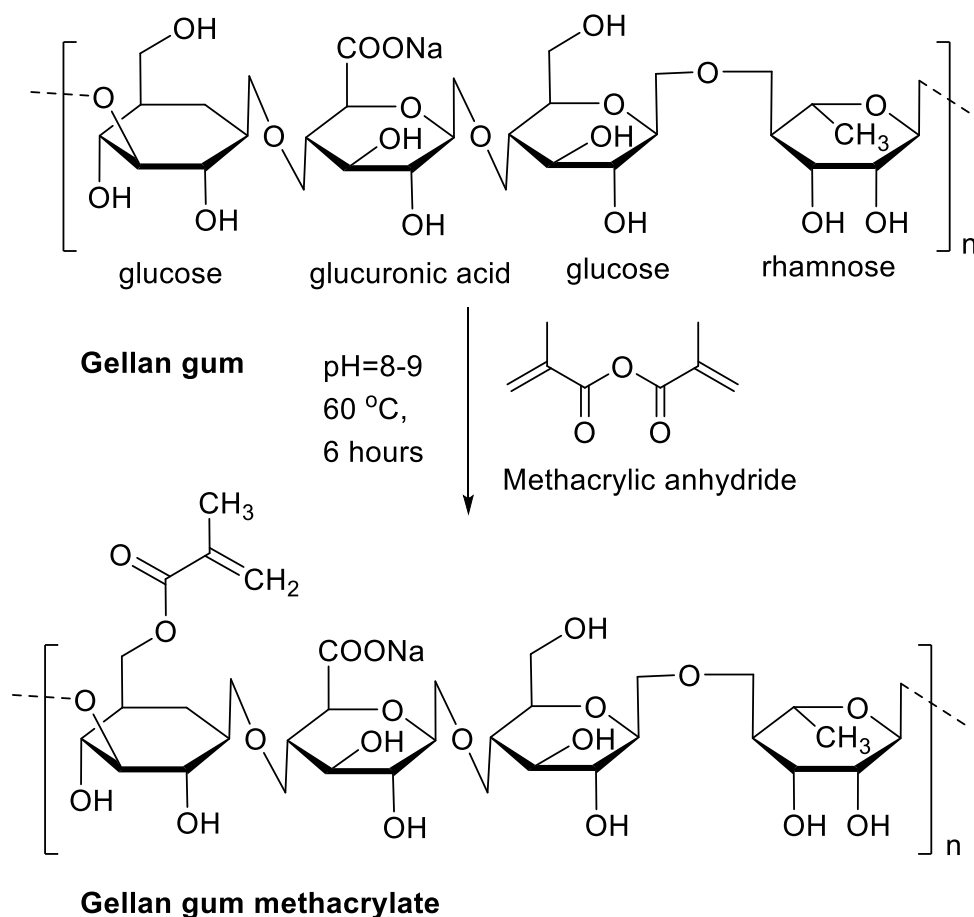


**Fig. 1.** Schematic illustration of the synthesis of GGMA.

## 2. Materials and methods

### 2.1. Synthesis and characterisation of modification degree of GGMA biomaterial inks

In this study, low acyl gellan gum (GG) was modified with a 15% degree of methacrylation (MA) (Fig. 1). GGMA with 15% MA was synthesised as follows. Low acyl gellan gum (Gelzan, purchased from Merck KGaA, USA) was purified to remove all divalent cations using the method reported elsewhere [23]. The purified GG was modified with functional methacrylate groups to enable photocrosslinking. Briefly, 1 g of GG was dissolved in 100 mL of DI water at 90 °C for 30 min, then cooled to 50 °C. Next, 8 mL of methacrylic anhydride (Merck KGaA, USA) was slowly added dropwise in the reaction mixture while stirring to maintain homogeneity for 3 h. Simultaneously, the pH was periodically adjusted to 8.5 with 5 M NaOH, and the reaction was continued for 6 h. GGMA was then transferred to dialysis membranes (11–14 kDa molecular weight-cutoff (MWCO) membrane (Spectra/Por, Repligen Corp., USA)) and dialysed against DI water for 5 days to remove any unreacted methacrylate anhydride. Water was changed 2–3 times a day until the solution became clear. The amount of unreacted methacrylic acid was monitored from dialysis water for 120 h using UV spectra (UV-3600 Plus, Shimadzu Corp., Japan) at a wavelength $350-500$ nm to confirm the complete removal of excess methacrylic acid from the product. The resulting GGMA was lyophilised and stored in a $-40$ °C dried refrigerator. The methacrylation degree of GG was quantified via $^{1}$H-NMR. The NMR spectra were recorded with the JEOL-500 MHz instrument (SCZ500R, JEOL Resonance, Japan) in $D_2O$ solvent. The spectra were acquired at RT.

### 2.2. Formulation of GGMA biomaterial inks and pre-crosslinking techniques

The GGMA inks were dissolved in DPBS solution with a presence of a photoinitiator (0.5% w/v, Irgacure 2959 purchased from Merck KGaA, USA) in an incubator at 37 °C. Three different GGMA concentrations were formulated: 1, 2 and 3% w/v and two pre-crosslinking methods were tested: low temperature (4 °C) and ionic crosslinking. Ionically pre-crosslinked biomaterial ink was prepared by using 0, 22.5, 45 or 90 mM $CaCl_2$ (final concentration). The pH of all GGMA inks with different formulations was adjusted to 7.5 to gain proper viscosity. The tested formulations were: $GGMA_{4°C}$ = GGMA at 4 °C, $GGMA_{22.5mM}$ = GGMA with 22.5 mM $CaCl_2$, $GGMA_{45mM}$ = GGMA with 45 mM $CaCl_2$ and $GGMA_{90mM}$ = GGMA with 90 mM $CaCl_2$. After that, the ink formulations were evaluated according to Fig. 2.

### 2.3. Prescreening of printability of GGMA biomaterial inks

The prescreening protocol has been previously reported [5]. A simple method to determine the printability of a biomaterial ink in extrusion-based bioprinting is to observe the filament formation and layer stacking ability. All the inks were loaded into a 10 mL cartridge and capped with a nozzle of 200 μm in diameter. The cartridge was clamped in a vertical position to minimise the variation of temperature. The biomaterial ink was extruded by an automatic dispenser, varying
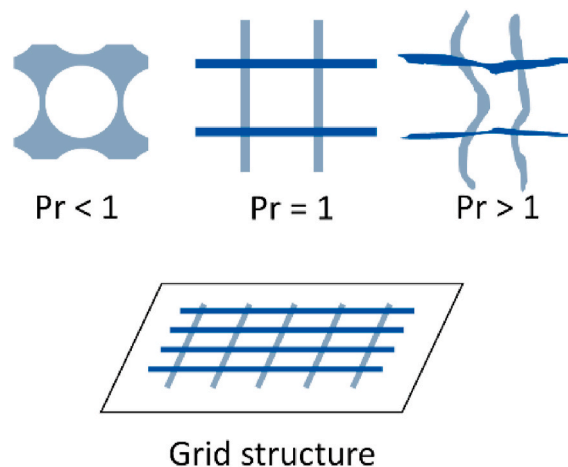


**Fig. 3.** Pore geometry evaluation and calculation of the printability (Pr) value. Ideally, Pr =1, indicating perfectly square-shaped pores.
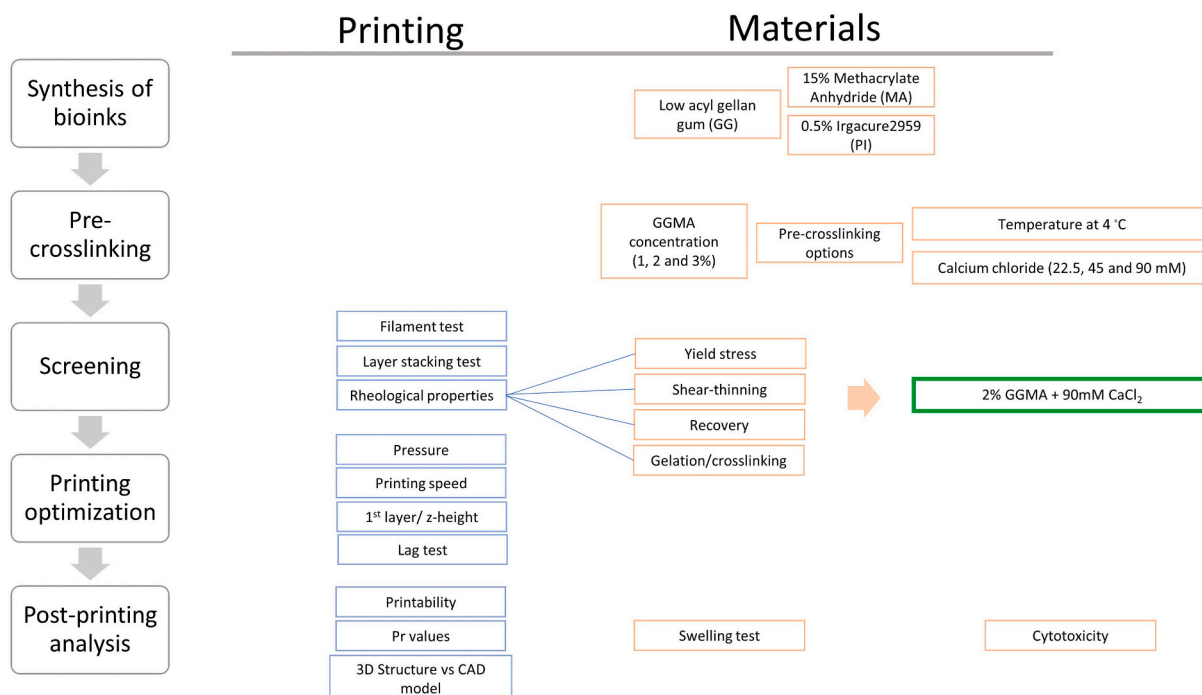


**Fig. 2.** Evaluation of GGMA biomaterial ink and development process.

the dispensing pressure between 0.1 and 2 bars and simultaneously observing the flow. The initial pressure was adjusted until the fibre started to flow, then slowly increased until the fibre was produced smoothly. The filament formation of different ink compositions was observed at RT and captured by a high-resolution mirrorless camera.

### 2.4. Rheological measurements of GGMA biomaterial inks

All rheological experiments were performed on a rotational rheometer (Discovery HR-2, TA Instruments Inc., USA) in parallel plate geometry (12 mm plate, 2.5 mm gap size). The temperature-dependent behaviour of GGMA was performed in flow mode (temperature sweep, 4−37 °C) with a constant shear rate (0.01 s$^{-1}$) at the rate of 2 °C/min (300 s soaking time). The results were plotted as a viscosity vs temperature graph.

For viscosity, yield stress, shear-thinning and recovery behaviour, the measurements were also performed in flow mode. The yield stress was determined using the shear rate-shear stress curve. The yield point was defined as the intersection point of the Y-axis at 0 shear rate in the shear stress-shear rate diagrams, indicating the point at which the material first started to flow. Shear-thinning was performed in flow mode with a shear rate ranging from 0.01−800 s$^{-1}$. Recovery behaviour measurements were performed to characterise the material's recovery behaviour by applying a low shear rate of 0.01 s$^{-1}$ for 200 s, followed by a high shear rate of 500 s$^{-1}$ for 100 s and finally, a low shear rate of 0.01 s$^{-1}$ for 200 s.

Gelation/crosslinking time evaluation was performed via *in situ* polymerisation using a rotational rheometer and external UV lamp (BlueWave 50 UV curing spot lamp, DYMAX Corp., USA) at 365 nm in wavelength and 25 mW/cm$^2$ in UV intensity. Viscoelasticity (storage and loss moduli, G' and G") was measured at RT as a function of time (500 s, UV lamp was activated at 100 s) while strain and frequency were kept constant at 1% and 1 Hz, respectively.

### 2.5. Shear-thinning coefficients of GGMA biomaterial inks

The Power-law regression model was applied to confirm the shear-thinning properties of the inks from the linear region of the viscosity-shear rate plots, calculated from Equation (1). The linear part of the curve from non-Newtonian region was chosen, where the viscosity drops with increasing shear rate.

$$\mu = K\gamma^{n-1} \qquad (1)$$

The flow index *n* relates to the shear-thinning abilities of the precursor, with n = 1 indicating Newtonian behaviour, n = 0.6 indicating weakly shear-thinning material, and n ≤ 0.2 meaning high shear-thinning properties and therefore good extrudability [3,24].

### 2.6. Quantitative evaluation of printability of GGMA biomaterial inks

Biomaterial inks were prepared as previously described, then loaded into a 10 mL cartridge (Optimum® syringe barrels, Nordson EFD, USA) and transferred in an incubator (37 °C) for 30 min to remove any air bubbles. Next, the cartridge was installed into a multi-material 3D bioprinter (BRINTER® 3D BIOPRINTER, Brinter Ltd., Finland). A 200 μm plastic UV shielded tapered nozzle (SmoothFlow™, Nordson EFD, USA) was attached to the cartridge and inserted into an air-pressure controlled Pneuma Tool print head (Fig. 4). To optimise the parameters, the pressure was set according to the previous prescreening test. Printing speed and print head temperature were constant at 8 mm/s and RT.

Biomaterial inks having ideal rheological properties, shear-thinning, and recovery behaviour produce coherent filaments, which are able to stack without merging [25,26]. Even though some of our GGMA ink candidates exhibited adequate results in both rheological and quantitative printability assessments, they could not be printed into 3D constructs. They either suffered from structure collapse, or upper layers started to merge with the lower layer. The next step for the practical printing assessment was to print grid patterns and apply a quantitative method to evaluate the shape of the printed pores using Equation (2):

$$Pr = \frac{\pi}{4} \cdot \frac{1}{C} = \frac{L^2}{16A}, \qquad (2)$$

in which C is the circularity of the enclosed pore, L means perimeter and A the pore area. We defined the biomaterial inks' printability (Pr) based on the squareness of the pores inside the grid structure. Pr value 1 indicates a perfect square shape. A CAD model for the square grids (20 x 20 x 0.4 mm$^3$) was drawn with AutoDesk Fusion 360 software and used as a standard for this assessment. Appropriately conditioned inks can produce smooth filaments with a constant width and stack into a 3D structure, yielding square pores in the fabricated construct with a Pr value of 1 (Fig. 3 and Fig. S4). On the other hand, poorly conditioned inks demonstrate the liquid-like or irregularly shaped filament, giving Pr value less than 1 or more than 1, respectively. The higher Pr value is a result of excessive pre-crosslinking. The lower Pr value is an indication of an inadequate degree of pre-crosslinking. To determine the Pr value of each ink with various printing parameter combinations, optical images of printed constructs were analysed in ImageJ to measure the circularity of the pores (n=5).

To obtain a perfect 3D construct, we determined pre-flow and post-flow delays via lag time calculation before and after the ink deposition. We found out that the flow of the inks showed delay after applying pressure and when changing a printing layer. This caused the structure to deform and collapse after fibre deposition in the subsequent layers (Fig. S3).
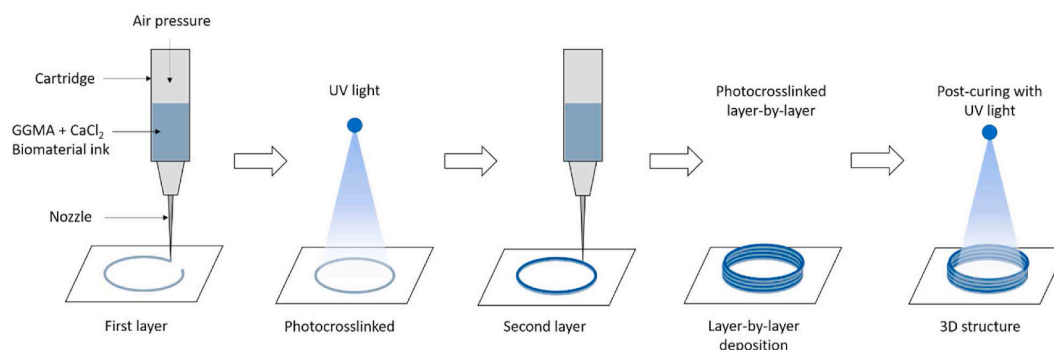


**Fig. 4.** Process flow of the extrusion-based 3D bioprinting process.

## 2.7. Printing accuracy and structural integrity of 3D printed GGMA hydrogels

After obtaining the best printable biomaterial ink formulation and optimal printing parameters, we assessed the structural integrity. We chose Nivea Creme (Nivea Creme, Beiersdorf Global AG, Germany) as a control printing material. It gave high geometric accuracy with minimal deviation compared to the CAD model [3,27]. The ink was printed into cylinders (10 mm in outer diameter) with different heights (1, 2.5 and 5 mm). Each structure was cured in a layer-by-layer fashion using the bioprinter's integrated UV/Vis LED module at a wavelength of 365 nm with 25 mW/cm$^2$ intensity for 10 s for each layer and 60 s for the post-curing process. The overview of the printing process is illustrated in Fig. 4. The dimensions of the cylinders were compared to the printed control structure to determine the printing accuracy. The structural integrity of each 3D printed structure was calculated as the ratio between dimensions of GGMA and control structure (1 = perfect structure, <1 = smaller in dimension, >1 = bigger dimensions than the control) [28].

For further in-depth structural analysis, the average mesh size and crosslinking density were determined from rheological measurement results [5,29]. The average mesh size ($\xi$, nm) calculation was applied using the storage moduli (G') of resulting hydrogels (the best formulation ink, 2% GGMA_90mM) at 0, 60, 120 and 180 s UV exposure time. Equation (3) estimates the average mesh size ($\xi$) of hydrogels at different exposure times:

$$(\xi) = \left(\frac{G'N}{RT}\right)^{-1/3},\tag{3}$$

where G' is the storage modulus of the hydrogel, N is the Avogadro constant (6.023 × 1023 mol$^{-1}$), R is the molar gas constant (8.314 JK$^{-1}$mol$^{-1}$), and T is the temperature (298 K).

Moreover, crosslinking density ($n_e$, mol/m$^3$) of the hydrogels were calculated using the storage modulus from the linear region of the frequency sweep test (a frequency range of 0.1–100 Hz). The data provided the total number of elastically active junction points in the network per unit of volume, using Equation (4).

$$n_e = \frac{G_e}{RT},\tag{4}$$

where $G_e$ is the average value of storage modulus from the linear region of oscillatory frequency sweep measurement.

## 2.8. Swelling of 3D printed GGMA hydrogels

The swelling ratio of the printed hydrogels was determined in DI water and cell culture media (Dulbecco's Modified Eagle's medium, DMEM). The GGMA was printed into cylinders with a height of 1 mm. Each experiment condition was tested with GGMA at a concentration of 2% GGMA_90mM. All samples were cured using 365 nm UV light at an intensity of 25 mW/cm$^2$ in a layer-by-layer fashion with 10 s exposure time followed by 60 s post-curing. The obtained hydrogels at zero time point were defined with a weight of $W_0$. The hydrogels were then immersed in the solution (DI water or DMEM) until equilibrium was reached and weighed ($W_s$). The swelling ratio was calculated at time points of 1, 2, 3, 4, 5, 24, 36 and 48 h using Equation (5).

$$Swelling\ Ratio = \frac{W_s - W_0}{W_0} \times 100\%.\tag{5}$$

## 3. Results

### 3.1. Synthesis and characterisation of modification of GGMA biomaterial inks

GGMA was functionalised by methacrylation of purified GG polymer.

The purity of dialysed GGMA was confirmed by UV absorption spectra (Fig. S1). The methacrylation degree of GGMA was characterised and verified by using $^1$H-NMR. The degree of methacrylation was calculated by comparing the integrated protons' peaks from methyl group on rhamnose ring of gellan gum (d =1.26 ppm) with a methyl group on the methacrylate moiety (d= 1.90 ppm) and vinylic protons on carbon-carbon double bond (d= 5.72 and 6.13 ppm) (Fig. S2).

### 3.2. Formulations and prescreening printability of GGMA biomaterial inks

GG and GGMA are capable of physical gelation via temperature change and ionic crosslinking. GGMA was prepared at different concentrations (1, 2 and 3% w/v). Initial testing screened the fibre-forming ability (in the air) of the pre-crosslinked GGMA. It was observed that GGMA solution alone at RT immediately formed a droplet after being extruded. Due to temperature-dependent viscosity, GGMA at 4 °C was more viscous and was able to form weak hydrogels. However, it could form a fibre only for a short time and was not able to maintain its shape after extruding from a nozzle. (The rheological data presented in the next section confirmed this phenomenon). According to Fig. 8, the ionic pre-crosslinking of GGMA was carried out by adding Ca$^{2+}$ ions and varying the concentration of GGMA (1, 2 and 3% w/v) and CaCl$_2$ solution (22.5, 45 and 90 mM). A mild ionic crosslinking of GGMA enabled the formation of a weak hydrogel, which was soft and extrudable. According to the results, all concentrations of GGMA with 45 or 90 mM of CaCl$_2$ (1% GGMA_45mM, 1% GGMA_90mM, 2% GGMA_45mM, 2% GGMA_90mM, 3% GGMA_45mM and 3% GGMA_90mM) were able to form coherent fibres that were assumed to be good candidates for 3D printing.

### 3.3. Rheological properties of GGMA inks and their pre-crosslinking methods

The evaluation of the rheological behaviour of GGMA was divided into three parts: yield stress, shear-thinning, and recovery behaviour. The shear-thinning profiles of each GGMA formulation were assessed to confirm the reliability of the prescreening method and to predict the extrudability. The Power-law model was applied to calculate the shear-
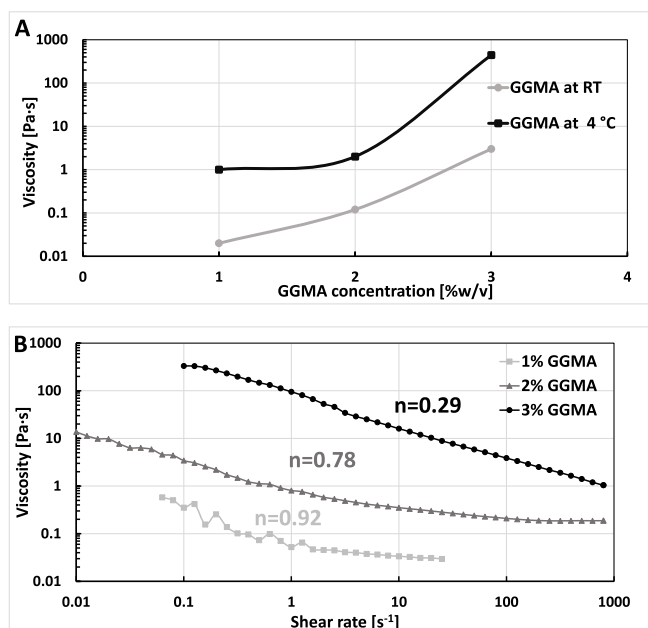


**Fig. 5.** A) The effect of temperature on GGMA at RT and 4 °C for various concentrations (1, 2 and 3%), B) Shear-thinning properties of 1, 2 and 3% GGMA concentrations at 4 °C.

thinning coefficients (*n* values). According to Fig. 5A and B, the viscosity of GGMA changed as a function of temperature. The results showed that 3% GGMA $_{4\ °C}$ without ionic crosslinking exhibited shear-thinning behaviour with decreasing viscosity as a function of increasing shear rate (*n* = 0.29). On the other hand, the prescreening method showed contradictory results. 3% GGMA $_{4\ °C}$ formed a temporary fibre in the air and lost its properties a few seconds after being extruded from a nozzle. 1 and 2% GGMA $_{4\ °C}$ exhibited Newtonian fluid behaviour.

Ionic pre-crosslinking resulted in the improvement of the shear-thinning behaviour, as shown in Fig. 6. 1% GGMA $_{22.5mM}$ and 1% GGMA $_{45mM}$ had a lot of variance due to the lack of viscosity and hence *n* values could not be obtained. 2% GGMA $_{22.5mM}$ was weakly shear-thinning (*n* = 0.55±0.01). Most of the 2 and 3% GGMA gels with 45 or 90 mM CaCl$_2$ (2% GGMA $_{45mM}$, 2% GGMA $_{90mM}$, 3% GGMA $_{45mM}$ and 3% GGMA $_{90mM}$) exhibited Non-Newtonian behaviour as the viscosity decreased as a function of increasing shear rate. The *n* values from the Power-law equation for 2% GGMA $_{45mM}$, 2% GGMA $_{90mM}$, 3% GGMA $_{45mM}$ and 3% GGMA $_{90mM}$ gels were 0.35±0.03, 0.10±0.03, 0.26±0.2 and 0.22±0.30, accordingly. In addition, 1% GGMA $_{90mM}$ and 3% GGMA $_{22.5mM}$ had some shear-thinning properties (*n* values were lower than 0.3).

Yield stress values of GGMA at different polymer and CaCl$_2$ concentrations were evaluated. According to Fig. 6, all concentrations of GGMA $_{22.5mM}$ have a low yield point, are low in viscosity and do not exhibit yield stress. In addition, 1% GGMA $_{45mM}$ cannot gain enough yield stress to show yielding behaviour. 2% and 3% GGMA with 45 or 90 mM CaCl$_2$ (2% GGMA $_{45mM}$, 2% GGMA $_{90mM}$, 3% GGMA $_{45mM}$ and 3% GGMA $_{90mM}$) showed a clear yield point. After the shear rate was increased, they exhibited Non-Newtonian behaviour and started to flow.

Recovery testing was performed to predict the recoverability of materials after being extruded from the print head. Ideally, GGMA should recover fast back to the initial viscosity level once printed on the substrate. According to Fig. 6, 1% GGMA $_{22.5mM}$ and 1% GGMA $_{45mM}$ were unable to be measured due to low viscosity, and the inks were completely splashed out from the geometry at a higher shear rate. In addition, 3% GGMA $_{90mM}$ was disintegrated and slipped out during the measurement because the ink appeared to be a hard and fragile hydrogel. Fig. 6 shows the recovery results for 1% GGMA $_{90mM}$, 2% GGMA $_{22.5mM}$, 2% GGMA $_{45mM}$, 2% GGMA $_{90mM}$, 3% GGMA $_{22.5mM}$ and 3% GGMA $_{45mM}$. Only 1% GGMA $_{90mM}$ and 2% GGMA $_{90mM}$ gels were able to rapidly recover their viscosity back to 90% of the original value after removing the shear. On the other hand, 2% GGMA $_{22.5mM}$, 2% GGMA $_{45mM}$, 3% GGMA $_{22.5mM}$, and 3% GGMA $_{45mM}$ did not recover their original viscosity quickly but required a longer recovery time (100 s for 2% GGMA) to reach back to their initial viscosity. The material properties of 3% GGMA changed permanently as a result of the high shear rate.

### 3.4. Gelation time of GGMA inks via in situ photo-rheology

As shown in Fig. 7, *in situ* photo-rheology was used to measure the gelation kinetics of GGMA at different concentrations after exposure to UV light. All GGMA concentrations rapidly gelated and crosslinked within 10 s and reached the maximum crosslinking state at 60 s. The concentration of GGMA had a significant effect on the final storage modulus, but the gelation time did not differ dramatically between various tested polymer concentrations.
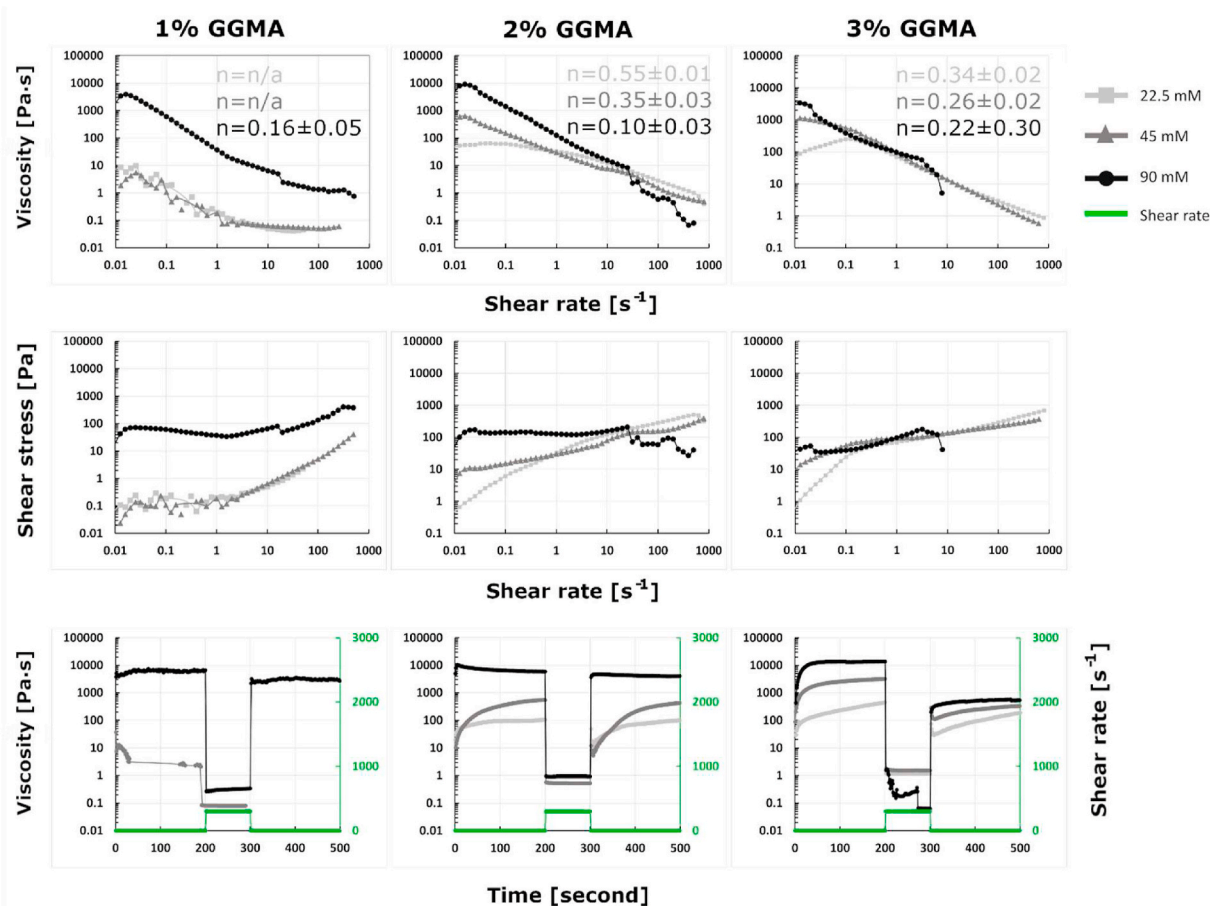


**Fig. 6.** Rheological properties: shear-thinning, yield stress and recovery for various GGMA and CaCl$_2$ concentrations at RT.
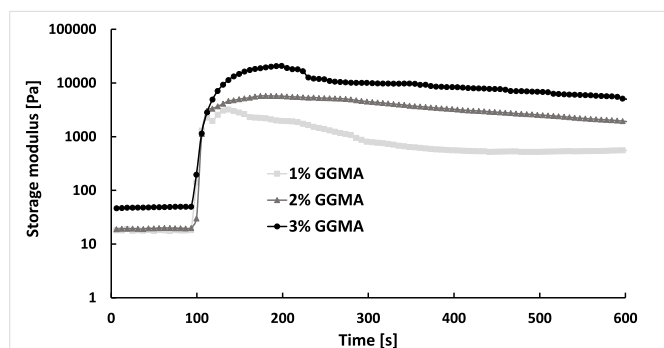
**Fig. 7.** In situ photorheology of 1%, 2% and 3% GGMA at RT.

### 3.5. Quantitative evaluation of printability of GGMA inks and ionic pre-crosslinking

Pr values were calculated for each combination of GGMA and $CaCl_2$ concentrations. Fig. 8 illustrates Pr values of GGMA with concentrations of 1, 2 and 3% w/v pre-crosslinked with $CaCl_2$ concentration of 0, 22.5, 45 or 90 mM. Ink is referred to as printable when the Pr value is 0.9–1.1 (Fig. 9). It was clear that GGMA without pre-crosslinking was unprintable at RT/4 °C even though 3% GGMA had the highest viscosity. Fig. 8 shows the relationship between various concentrations of GGMA mixed with various concentrations of $CaCl_2$. Pr value of GGMA_22.5mM could not be quantified at all due to insufficient ionic crosslinking. The Pr value of 1% GGMA_45mM could not be defined due to poor gelation. For 1% GGMA_90mM, Pr value was 0.78±0.4.

On the other hand, 3% GGMA_90mM appeared as overgelated ink due to excessive ionic crosslinking. It required high pressure to be extruded and formed a tough hydrogel inside the nozzle, resulting in variable-sized printed fibre and irregularly shaped pores (Pr = 1.1± 0.3). Printability of 2% GGMA_90mM and 3% GGMA_45mM fell into the proper region of printability, being 0.97 and 1.1, respectively. However, 2% GGMA produced smooth and coherent grid structures as compared to the crooked and uneven shape of 3% GGMA_45mM grids. 2% GGMA_45mM with the value of 0.82±0.04 was also printable but was not viscous enough to maintain the grid shape.

### 3.6. Printing accuracy and structural integrity

The CAD models of cylinders had a wall height of 1, 2.5 or 5 mm and consisted of 6, 16 or 33 layers. The printed GGMA structures were compared to the printed control structure to calculate the %error and
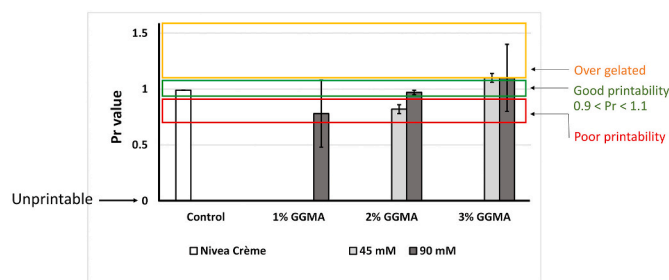
structural integrity (Fig. 10). Table 1 shows all measured dimensions of GGMA 3D structures: cylinder height, diameter (inner and outer) and wall thickness.

The average mesh sizes ($\xi$) and crosslinking densities ($n_e$) were calculated using Equations (3) and (4). The calculated parameters can be found in the supporting information (Table S1). Crosslinked hydrogels (2% GGMA_90mM) with the 180 s of UV exposure time had a smaller mesh size than crosslinked hydrogels with 60 s or no exposure. On the other hand, the longest UV exposure time (180 s) yielded the highest value of crosslinking density.



**Fig. 9.** The calculated Pr values for Nivea Creme (control) and various GGMA formulations with different amounts of $CaCl_2$ pre-crosslinking.
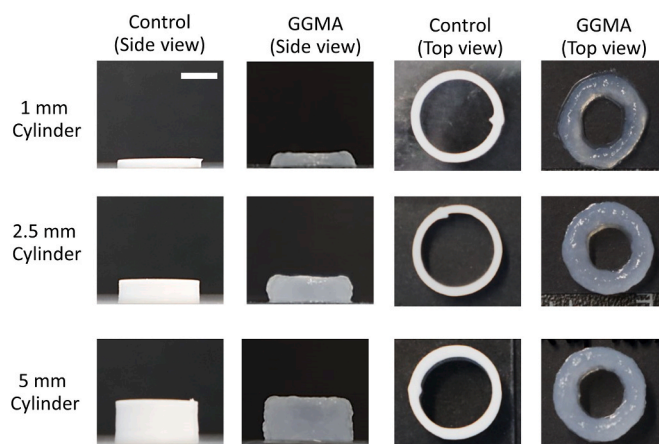


**Fig. 10.** Side-views and top-views of printed cylinders for the evaluation of printing accuracy and structural integrity, The scale bar = 5 mm.
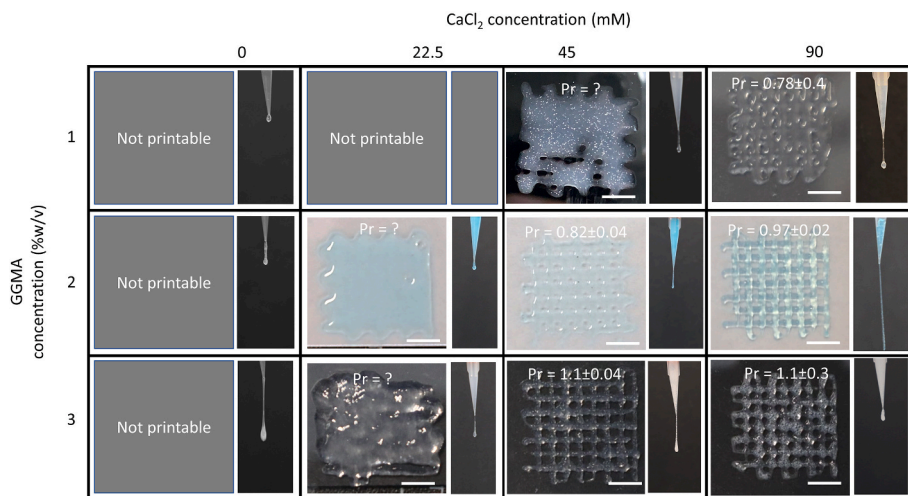


**Fig. 8.** The fibre formation results and printed grid structures of GGMA/$CaCl_2$ inks in terms of printability at RT. The scale bar is 5 mm.

**Table 1**
Dimensions of the printed cylinders, including the percentage error, compared to the control cylinder and structural integrity ratio.

| 1 mm cylinder [6 layers] | Control dimensions [mm] | GGMA dimensions [mm] | Error [%] | Structural integrity ratio |
|---|---|---|---|---|
| height | 1.3±0.1 | 1.7±0.2 | 30.7±5.1 | 1.31±0.05 |
| outer diameter | 11.0±0.2 | 11.2±0.2 | 1.8±0.2 | 1.02±0.01 |
| inner diameter | 8.80±0.2 | 6.5±0.3 | 26.2±2.7 | 0.73±0.04 |
| wall thickness | 1.2±0.1 | 3.0±0.1 | 150.7±10.8 | 2.50±1.30 |
| 2.5 mm cylinder [16 layers] | Control dimensions [mm] | GGMA dimensions [mm] | Error [%] | Structural integrity ratio |
| height | 3.2±0.1 | 3.7±0.3 | 15.6±3.7 | 1.15±0.06 |
| outer diameter | 11.0±0.1 | 11.7±0.2 | 6.3±1.5 | 1.06±0.01 |
| inner diameter | 8.8±0.2 | 6.2±0.1 | 28.5±2.8 | 0.70±0.04 |
| wall thickness | 1.2±0.2 | 3.1±0.1 | 158.7±12.5 | 2.58±0.28 |
| 5 mm cylinder [33 layers] | Control dimensions [mm] | GGMA dimensions [mm] | Error [%] | Structural integrity ratio |
| height | 5.8±0.1 | 7.2±0.2 | 24.21±1.2 | 1.24±0.02 |
| outer diameter | 11.2±0.2 | 11.2±0.1 | 10.7±5.8 | 1.04±0.02 |
| inner diameter | 8.4±0.2 | 5.6±0.2 | 33.3±5.3 | 0.66±0.01 |
| wall thickness | 1.4±0.2 | 3.2±0.1 | 128.5±7.2 | 2.28±0.22 |

### 3.7. Swelling of the 3D printed structures

The printed structures were immersed in DI water and DMEM for 48 h and periodically weighted at different time points (Figs. S5 and S6). Samples (in DI water and DMEM) without UV post-curing were completely disintegrated after 30 min in an incubator at 37 °C. As shown in Fig. 11, samples immersed in water quickly absorbed water into the structures after only 30 min, resulting in enormous swelling up to almost 200% at the 5-h time point. The swelling saturated after 10 h immersion in water, then slowly decreased after 24 h (% swelling reduced to ~100%) and became steady until 48 h. When immersed in DMEM, the samples gradually shrank and reached the equilibrium stage after 5 h. The swelling ratio of the samples in DMEM stayed constant until the end of the swelling study.

## 4. Discussion

In this study, we have developed a two-step crosslinking technique using ionic pre-crosslinking together with photocrosslinking to enhance



**Fig. 11.** Swelling behaviour of the printed GGMA structures. The samples were immersed in two different media: deionised water and DMEM.

the printability of GGMA biomaterial ink. Hence, we ended up using ionic $CaCl_2$ crosslinking of GGMA precursors by tuning the polymer and $Ca^{2+}$ concentrations. While the pre-crosslinking technique using $CaCl_2$ is a well-known and widely used approach for alginate and nanocellulose inks, it has not been previously used for GGMA biomaterial inks [30,31]. Also, the mixture of gellan gum and calcium ions has been reported to increase the elastic modulus of the resulting bulk hydrogels [20,32]. However, the combination has not been studied from the 3D printability perspective. The incorporation of $Ca^{2+}$ into GGMA improves the viscosity of the inks, even with low GGMA concentrations, and enables them to sustain the 3D shape before photocrosslinking. However, the tuning of the $Ca^{2+}$ concentration needs to be meticulous, as incorrect $Ca^{2+}$ amount can lead to poor printability (either too liquid or too viscous ink) [3].

To optimise the printing outcome, we evaluated the effect of different ratios of GGMA and $CaCl_2$ on printing results. After applying ionic pre-crosslinking, weak hydrogels were obtained. They were soft and extrudable and maintained their shape after being deposited from the nozzle in the printing process. Photocrosslinking was applied layer-by-layer to turn the weak hydrogels into true hydrogels with stable 3D shapes. We combined several assessment methods (Fig. 2) into a step-by-step process to measure the true printability of the inks [25]: pre-screening of extrudability (fibre formation), rheological measurements (shear-thinning, yield stress and recovery behaviour), and quantification of printability (Pr value) from the printed grids [33].

Shear-thinning properties especially have been used in several research studies to show the printability of novel biomaterial inks [34, 35]; however, those characteristics alone cannot guarantee that the inks can be successfully printed. According to our prescreening printability data, GGMA should have been printable at room temperature (RT) if the polymer concentration was high enough. However, the experimental printing tests showed otherwise. Without pre-crosslinking, GGMA inks at RT could not be printed into 3D structures as they did not form fibres nor had appropriate rheological behaviour. On the contrary, GGMA precursors at low temperature (4 °C) showed good shear-thinning properties ($n$ value was lower than 0.3) but behaved like liquid after being deposited on the substrate. The explanation for this result could be that the GGMA precursor was cooled in the syringe, but the temperature suddenly rose after the printed filament was exposed to the room temperature on the printing substrate. Hence, the viscosity of the GGMA ink had to be improved by applying ionic pre-crosslinking.

We found that $Ca^{2+}$ played an essential role in determining the viscosity and shear-thinning coefficients of GGMA inks. The viscosity changed as a function of the $CaCl_2$ concentration. These pre-crosslinked inks also had a high shape fidelity after extrusion. However, GGMA (1–3% w/v) pre-crosslinked with a low concentration of $CaCl_2$ (22.5 mM) had poor printability and could not form a consistent fibre. Their rheological profiles also supported our findings of the poor printability as the samples could not recover back to their initial viscosity after the high shear rate, suggesting an insufficient ionic pre-crosslinking. According to the results, it is apparent that low polymer concentration requires more $Ca^{2+}$ pre-crosslinking to gain enough viscosity for 3D printing, while inks with higher polymer concentration can be printed with lower $Ca^{2+}$ concentration. In general, pre-crosslinked GGMA inks with $Ca^{2+}$ displayed rapid viscosity recovery after removing the high shear rate. The recovery test results also showed that a higher $Ca^{2+}$ amount in GGMA ink improved recovery behaviour in all polymer concentrations, except in 3% $GGMA_{90mM}$. 3% GGMA_90 mM appeared as solid hydrogel and was not extrudable. In addition, according to Cao et al. [35] and Coutinho et al. [20], even a 90 mM concentration of $CaCl_2$ as a crosslinker barely affects the ink's biocompatibility and shows no significant effect on the viability of encapsulated cells (both fibroblasts and neural cells) [31].

Photorosslinking kinetics of the GGMA inks were monitored using *in situ* photorheology. As observed from Fig. 7, the storage moduli of all GGMA concentrations immediately increased after exposure to the UV
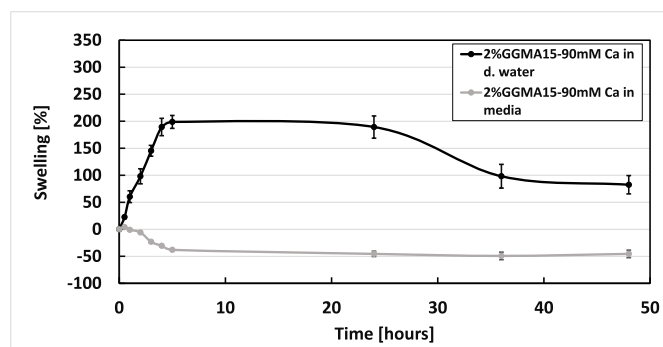
light. The storage moduli increased dramatically as a function of the curing time and reached a plateau after 60 s. The possible reason for the plateaued curve is that the precursors became fully crosslinked, as explained in the literature [36]. The exposure times for the layer-by-layer curing during printing and post-curing phase were chosen to match the conditions of the *in situ* photorheology, i.e. 25 mW/cm$^2$ intensity for 10 s for each layer and 60 s for the post-curing process.

Quantitative printability evaluation was defined via Pr value, which other researchers have used as a guideline for the selection of bio-printing parameters [25,26,37,38]. According to Ouyang et al. [25], the Pr value should be in the range of 0.9–1.1. In our study, the printability improved when the concentration increased for either GGMA or CaCl$_2$. In the inks with low Pr values (less than 0.8), the pores inside the grid structures were fused and were evaluated as having poor printability. On the other hand, in the inks with high Pr values (more than 1.1), the square shape of the pores deviated from the CAD model and were also assigned as having poor printability.

In addition to the Pr value evaluation, the dimensions of the printed 3D structures were measured to estimate the printing error (i.e., the deviation from the control structure dimensions) and structural integrity. Nivea Creme was chosen as a control for the evaluation because it exhibits good fibre formation. The formed fibres are highly consistent and maintain their shape without merging/breaking during the printing. The grid constructs attach well to the glass slide and keep the shape of a crosshatch [3]. Also, the printed Nivea Creme structures have only a slight deviation from the CAD model and thus represent a perfect example of material behaviour during the printing process. The structural analysis of printed 3D structures and comparison to control samples was adopted from Gao et al. [28]. According to the structural integrity analysis, all GGMA structures ended up being a bit bigger than the control structures in all dimensions because the rheological recovery degree of GGMA was only 70–90%, and the structural integrity ratio was more than 1.0. The extruded fibres on the glass substrate were swollen and had pronounced dimensions in every layer. The wall thickness had the highest deviation, and the deviation increased as a function of the number of the printed layers. The wall thickness of the GGMA cylinders was considerably more prominent than in the control cylinders as the GGMA fibres spread, resulting in a high deviation in the inner diameter. Another reason for the deviation could be the slanted cylinder walls, resulting in measurement errors in the wall heights. The average mesh size and crosslinking density will not directly explain the pore size of hydrogels but will provide more structural insight since pore size is related to mesh size [29]. In addition, the average mesh size values reflect the crosslinking density (smaller mesh sizes lead to higher crosslinking density). These values are crucial in evaluating the suitability of these photocrosslinked hydrogels for biomedical applications. The average mesh size of 2% GGMA_90 mM was around 10–15 nm, which is comparable to other natural hydrogels having a mesh size of 5–100 nm [39]. The size range of 5–100 nm allows the exchange of small molecules, such as nutrients and growth factors, while the flow of non-covalently entrapped larger molecules may be hindered. Anyhow, most proteins and peptides in human cells can easily diffuse through our GGMA gels since their diameter is less than 7 nm [40].

The swelling/shrinking behaviour is normally studied to confirm the mechanical stability of hydrogels in aqueous media [33]. The printed GGMA structures shrank immediately in the DMEM solution, suggesting they were influenced by the cations in the solution. On the contrary, the samples in water swell and quickly uptook the water, losing their integrity over time because DI water has no ions. These results are supported by the previous studies of alginate and gellan gum hydrogels. The shrinking phenomenon has also been observed by Coutinho et al. [20] when the hydrogels were immersed in media containing Ca$^{2+}$. According to the swelling test of bulk hydrogels done by Xu et al. [32] and Coutinho et al. [20], solid GGMA hydrogels swell at a slower rate compared to our printed GGMA structures. This difference results from the fact that the surface area of hydrogels strongly influences the

swelling kinetics. Our cylinder-shaped printed structures have a higher surface area than the solid bulk hydrogels and thus swell faster.

## 5. Conclusions

In this study, we successfully developed a two-step crosslinking technique to achieve 3D printed structures from GGMA biomaterial inks with extrusion-based bioprinting. With a sufficient amount of calcium chloride precrosslinker, GGMA transformed from a liquid precursor to a weak printable hydrogel, which could be further photocrosslinked into a true hydrogel with good shape fidelity. The printing parameters were optimised through stepwise characterisation of printability and rheological properties. According to the prescreening results, viscosity data and shear-thinning coefficients alone cannot guarantee the success of 3D printing. They do not predict the actual printing outcome, which is governed by gravitational forces and the surface properties of the printing substrate. However, the rheological data was valuable to predict the extrudability of the inks out from a nozzle. Our ink optimisation process showed that the polymer and calcium chloride concentration affected the printability of GGMA inks. We found that out of the studied combinations, 2% GGMA_90mM and 3% GGMA_45mM were best in printing. 2% GGMA_90mM was selected as the best combination, and 3D printed cylinders were achieved with the height of 1, 2.5 and 5 mm. However, the printed outcome still lacked high resolution compared to the control samples and the CAD model. The study highlights that the two-step crosslinking approach is an effective way to convert unprintable GGMA ink into stackable material capable of forming 3D constructs. Our qualitative and quantitative analyses can be applied to other bioinks/biomaterial inks in the field of biofabrication, as well.

## CRediT authorship contribution statement

**Hatai Jongprasitkul:** Conceptualization, Methodology, Investigation, Formal analysis, Writing – original draft, Visualization, Validation. **Sanna Turunen:** Conceptualization, Methodology, Investigation, Formal analysis, Validation, Writing – original draft, Supervision. **Vijay Singh Parihar:** Conceptualization, Methodology, Resources, Formal analysis, Validation, Writing – review & editing, Data curation, Supervision. **Minna Kellomäki:** Conceptualization, Methodology, Funding acquisition, Project administration, Writing – review & editing, Supervision.

## Declaration of competing interest

The authors declare that they have no known competing financial interests or personal relationships that could have appeared to influence the work reported in this paper.

## Acknowledgement

## Appendix A. Supplementary data

Supplementary data to this article can be found online at https://doi.org/10.1016/j.bprint.2021.e00185.

# References

[1] I.T. Ozbolat, M. Hospodiuk, Current advances and future perspectives in extrusion-based bioprinting, Biomaterials 76 (2016) 321–343, https://doi.org/10.1016/j.biomaterials.2015.10.076.

[2] M. Amr, M. Counts, J. Kernan, A. Mallah, J. Mendenhall, B. Van Wie, N. Abu-lail, B. A. Gozen, Bioprinting 3D printed , mechanically tunable , composite sodium alginate , gelatin and Gum Arabic (SA-GEL-GA) scaffolds, Bioprinting 22 (2021), e00133, https://doi.org/10.1016/j.bprint.2021.e00133.

[3] N. Paxton, W. Smolan, T. Böck, F. Melchels, J. Groll, T. Jungst, Proposal to assess printability of bioinks for extrusion-based bioprinting and evaluation of rheological properties governing bioprintability, Biofabrication 9 (2017), 44107, https://doi.org/10.1088/1758-5090/aa8dd8.

[4] C.J. Ferris, K.J. Gilmore, S. Beirne, D. McCallum, G.G. Wallace, M. Het Panhuis, Bio-ink for inkjet printing of living cells, Tech. Proc. 2013 NSTI Nanotechnol. Conf. Expo, NSTI-Nanotech 2013 2 (2013) 261–264.

[5] H. Jongprasitkul, S. Turunen, V.S. Parihar, S. Annurakshita, M. Kellomäki, Photocross-linkable methacrylated polypeptides and polysaccharides for casting, injecting, and 3D fabrication, Biomacromolecules 22 (2021) 481–493, https://doi.org/10.1021/acs.biomac.0c01322.

[6] M.K. Włodarczyk-Biegun, A. del Campo, 3D bioprinting of structural proteins, Biomaterials 134 (2017) 180–201, https://doi.org/10.1016/j.biomaterials.2017.04.019.

[7] S.A. Bencherif, A. Srinivasan, F. Horkay, J.O. Hollinger, K. Matyjaszewski, N. R. Washburn, Influence of the degree of methacrylation on hyaluronic acid hydrogels properties, Biomaterials 29 (2008) 1739–1749, https://doi.org/10.1016/j.biomaterials.2007.11.047.

[8] A. Isaacson, S. Swioklo, C.J. Connon, 3D bioprinting of a corneal stroma equivalent, Exp. Eye Res. 173 (2018) 188–193, https://doi.org/10.1016/j.exer.2018.05.010.

[9] H. Li, S. Liu, L. Li, Rheological study on 3D printability of alginate hydrogel and effect of graphene oxide, Int. J. Bioprinting. 2 (2016) 54–66, https://doi.org/10.18063/IJB.2016.02.007.

[10] L.E. Bertassoni, M. Cecconi, V. Manoharan, M. Nikkhah, J. Hjortnaes, A.L. Cristino, G. Barabaschi, D. Demarchi, M.R. Dokmeci, Y. Yang, A. Khademhosseini, Hydrogel bioprinted microchannel networks for vascularization of tissue engineering constructs, Lab Chip 14 (2014) 2202–2211, https://doi.org/10.1039/c4lc00030g.

[11] M.E. Cooke, D.H. Rosenzweig, The rheology of direct and suspended extrusion bioprinting, APL Bioeng 5 (2021), 011502, https://doi.org/10.1063/5.0031475.

[12] J. Groll, J.A. Burdick, D.W. Cho, B. Derby, M. Gelinsky, S.C. Heilshorn, T. Jüngst, J. Malda, V.A. Mironov, K. Nakayama, A. Ovsianikov, W. Sun, S. Takeuchi, J. J. Yoo, T.B.F. Woodfield, A definition of bioinks and their distinction from biomaterial inks, Biofabrication 11 (2019), 013001, https://doi.org/10.1088/1758-5090/aaec52.

[13] T.M. Robinson, S. Talebian, J. Foroughi, Z. Yue, C.D. Fay, G.G. Wallace, Fabrication of aligned biomimetic gellan gum-chitosan microstructures through 3D printed microfluidic channels and multiple in situ cross-linking mechanisms, ACS Biomater. Sci. Eng. 6 (2020) 3638–3648, https://doi.org/10.1021/acsbiomaterials.0c00260.

[14] C.J. Ferris, K.J. Gilmore, G.G. Wallace, M. In Het Panhuis, Modified gellan gum hydrogels for tissue engineering applications, Soft Matter 9 (2013) 3705–3711, https://doi.org/10.1039/c3sm27389j.

[15] H.H. Mishbak, G. Cooper, P.J. Bartolo, Development and characterization of a photocurable alginate bioink for three-dimensional bioprinting, Int. J. Bioprinting. 5 (2019) 12–26, https://doi.org/10.18063/IJB.V5I2.189.

[16] V.H.M. Mouser, F.P.W. Melchels, J. Visser, W.J.A. Dhert, Yield stress determines bioprintability of hydrogels based on gelatin-methacryloyl and gellan gum for cartilage bioprinting, Biofabrication 8 (2016) 1–24, https://doi.org/10.1088/1758-5090/8/3/035003.

[17] D. Wu, Y. Yu, J. Tan, L. Huang, B. Luo, L. Lu, C. Zhou, 3D bioprinting of gellan gum and poly (ethylene glycol) diacrylate based hydrogels to produce human-scale constructs with high-fidelity, Mater. Des. 160 (2018) 486–495, https://doi.org/10.1016/j.matdes.2018.09.040.

[18] S. Pacelli, P. Paolicelli, I. Dreesen, S. Kobayashi, A. Vitalone, M.A. Casadei, Injectable and photocross-linkable gels based on gellan gum methacrylate: a new tool for biomedical application, Int. J. Biol. Macromol. 72 (2015) 1335–1342, https://doi.org/10.1016/j.ijbiomac.2014.10.046.

[19] J. Hazur, R. Detsch, E. Karakaya, J. Kaschta, J. Teßmar, D. Schneidereit, O. Friedrich, D.W. Schubert, A.R. Boccaccini, Improving alginate printability for biofabrication: establishment of a universal and homogeneous pre-crosslinking technique, Biofabrication 12 (2020), 045004, https://doi.org/10.1088/1758-5090/ab98e5.

[20] D.F. Coutinho, S.V. Sant, H. Shin, J.T. Oliveira, M.E. Gomes, N.M. Neves, A. Khademhosseini, R.L. Reis, Modified Gellan Gum hydrogels with tunable physical and mechanical properties, Biomaterials 31 (2010) 7494–7502, https://doi.org/10.1016/j.biomaterials.2010.06.035.

[21] S.R. Van Tomme, G. Storm, W.E. Hennink, In situ gelling hydrogels for pharmaceutical and biomedical applications, Int. J. Pharm. 355 (2008) 1–18, https://doi.org/10.1016/j.ijpharm.2008.01.057.

[22] J. Silva-Correia, J. Bavan, V. Vindigni, T.H. Silva, J.M. Oliveira, G. Abatangelo, R. L. Reis, Biocompatibility evaluation of ionic- and photo-crosslinked methacrylated gellan gum hydrogels: in vitro and in vivo study, Adv. Healthc. Mater. 2 (2013) 568–575, https://doi.org/10.1002/adhm.201200256.

[23] D.M. Kirchmajer, B. Steinhoff, H. Warren, R. Clark, M. In Het Panhuis, Enhanced gelation properties of purified gellan gum, Carbohydr. Res. 388 (2014) 125–129, https://doi.org/10.1016/j.carres.2014.02.018.

[24] E. Reina-Romo, S. Mandal, P. Amorim, V. Bloemen, E. Ferraris, L. Geris, Towards the experimentally-informed in silico nozzle design optimization for extrusion-based bioprinting of shear-thinning hydrogels, Front. Bioeng. Biotechnol. 9 (2021) 1–14, https://doi.org/10.3389/fbioe.2021.701778.

[25] L. Ouyang, R. Yao, Y. Zhao, W. Sun, Effect of bioink properties on printability and cell viability for 3D bioplotting of embryonic stem cells, Biofabrication 8 (2016) 1–12, https://doi.org/10.1088/1758-5090/8/3/035020.

[26] G. Gillispie, P. Prim, J. Copus, J. Fisher, A.G. Mikos, J.J. Yoo, A. Atala, S.J. Lee, Assessment methodologies for extrusion-based bioink printability, Biofabrication 12 (2020), 022003, https://doi.org/10.1088/1758-5090/ab6f0d.

[27] L. Horvath, Y. Umehara, C. Jud, F. Blank, A. Petri-Fink, B. Rothen-Rutishauser, Engineering an in vitro air-blood barrier by 3D bioprinting, Sci. Rep. 5 (2015) 7974, https://doi.org/10.1038/srep07974.

[28] T. Gao, G.J. Gillispie, J.S. Copus, A.K. Pr, Y.-J. Seol, A. Atala, J.J. Yoo, S.J. Lee, Optimization of gelatin alginate composite bioink printability using rheological parameters: a systematic approach, Biofabrication 10 (2018), 34106, https://doi.org/10.1088/1758-5090/aacdc7.

[29] J. Karvinen, T.O. Ihalainen, M.T. Calejo, I. Jönkkäri, M. Kellomäki, Characterization of the microstructure of hydrazone crosslinked polysaccharide-based hydrogels through rheological and diffusion studies, Mater. Sci. Eng. C 94 (2019) 1056–1066, https://doi.org/10.1016/j.msec.2018.10.048.

[30] A.A. Aldana, F. Valente, R. Dilley, B. Doyle, Development of 3D bioprinted GelMA-alginate hydrogels with tunable mechanical properties, Bioprinting 21 (2021), e00105, https://doi.org/10.1016/j.bprint.2020.e00105.

[31] T. Gonzalez-Fernandez, A.J. Tenorio, K.T. Campbell, E.A. Silva, J.K. Leach, Alginate-based bioinks for 3D bioprinting and fabrication of anatomically accurate bone grafts, Tissue Eng. (2021) 1–14, https://doi.org/10.1089/ten.tea.2020.0305.

[32] Z. Xu, Z. Li, S. Jiang, K.M. Bratlie, Chemically modified gellan gum hydrogels with tunable properties for use as tissue engineering scaffolds, ACS Omega 3 (2018) 6998–7007, https://doi.org/10.1021/acsomega.8b00683.

[33] A. Ribeiro, M.M. Blokzijl, R. Levato, C.W. Visser, M. Castilho, W.E. Hennink, T. Vermonden, J. Malda, Assessing bioink shape fidelity to aid material development in 3D bioprinting, Biofabrication 10 (2018), 014102, https://doi.org/10.1088/1758-5090/aa90e2.

[34] E.A. Kiyotake, A.W. Douglas, E.E. Thomas, S.L. Nimmo, M.S. Detamore, Development and quantitative characterization of the precursor rheology of hyaluronic acid hydrogels for bioprinting, Acta Biomater. 95 (2019) 176–187, https://doi.org/10.1016/j.actbio.2019.01.041.

[35] N. Cao, X.B. Chen, D.J. Schreyer, Influence of calcium ions on cell survival and proliferation in the context of an alginate hydrogel, ISRN Chem. Eng. (2012), 516461, https://doi.org/10.5402/2012/516461.

[36] K.S. Lim, J.H. Galarraga, X. Cui, G.C.J. Lindberg, J.A. Burdick, T.B.F. Woodfield, Fundamentals and applications of photo-cross-linking in bioprinting, Chem. Rev. 120 (2020) 10662–10694, https://doi.org/10.1021/acs.chemrev.9b00812.

[37] P. Zhuang, W.L. Ng, J. An, C.K. Chua, L.P. Tan, Layer-by-layer ultraviolet assisted extrusion-based (UAE) bioprinting of hydrogel constructs with high aspect ratio for soft tissue engineering applications, PLoS One 14 (2019) 1–21, https://doi.org/10.1371/journal.pone.0216776.

[38] A. Schwab, R. Levato, M. D'Este, S. Piluso, D. Eglin, J. Malda, Printability and shape fidelity of bioinks in 3D bioprinting, Chem. Rev. 120 (2020) 11028–11055, https://doi.org/10.1021/acs.chemrev.0c00084.

[39] J. Li, D.J. Mooney, Designing hydrogels for controlled drug delivery, Nat. Rev. Mater. 1 (2016) 1–18, https://doi.org/10.1038/natrevmats.2016.71.

[40] E.R. Aurand, K.J. Lampe, K.B. Bjugstad, Defining and designing polymers and hydrogels for neural tissue engineering, Neurosci. Res. 72 (2012) 199–213, https://doi.org/10.1016/j.neures.2011.12.005.